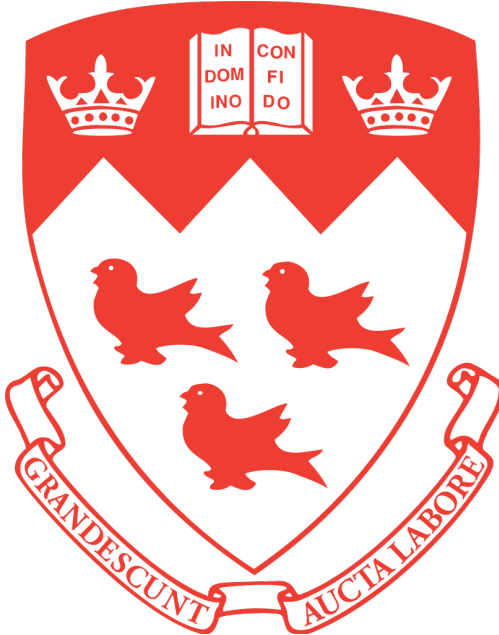


X-ray flares detection and analysis using Bayesian blocks algorithms

Supervised by Professor Daryl Haggard

Nicolas Choux

The report presented for the research class
PHYS479: Honours Research Project



Department of Physics

McGill University

Canada

August 29, 2016

Abstract

Sagittarius A* (Sgr A*) is the supermassive black hole that resides in the center of our galaxy. It emits frequent X-ray flares, which are detected by the Chandra X-ray Observatory once per day on average. The goal for this project is to search for X-ray flares from Sgr A*. Employing 900 ks of data from the Chandra X-ray Observatory, collected between May 2013 and October 2014, we seek flares using Bayesian blocks functions based on the algorithms of Jeffrey D. Scargle. We present the Bayesian blocks analysis of 26 observations containing the two enormous flares found by Daryl Haggard's team in September 2013 and October 2014 with peak count rates of $0.87 \pm 0.07 \text{counts/s}$ and $0.45 \pm 0.04 \text{count/s}$ as well as 13-16 faint flares among which 5-8 of them were not found in a previous analysis of G.Ponti [2].

1 Introduction

Black holes are objects in the universe from which nothing, not even light, can escape. The 4-million-solar-mass supermassive black hole sitting at the center of our Galaxy, at a distance of 26,000 light years from Earth, is called Sagittarius A* (Sgr A*). Many objects are orbiting Sgr A*. The accretion disk, the hot area where orbits all these objects, is a hive of activity that we want to understand. The photons emitted from this hot active region form a quiescent¹ signal perturbed sometimes by patterns of small and bigger bursts of photons. The light coming from SgrA* is emitted in different frequency domains (X-ray, radio, IR, submillimiter).

After more than 10 years studying Sgr A*, we still don't know clearly what causes this variability. However there exist some theories. One of the theories since 2012, explained in NASA's article [6], states that these flares occurring on average once a day could be caused by asteroids falling into Sgr A*. There would be hundreds of trillions of them around the supermassive black hole (PanelA of Fig-

ure 1). Once an asteroid enters the very hot region, the tidal forces from the black hole turn the asteroid into pieces.(PanelB of Figure 1) As it passes through the hot thin gas there, the friction heats the fragments to X-ray-emitting temperatures creating a X-ray flare(PanelC).

On September, 14 2013, the brightest X-ray flare ever observed was discovered (see NASA's Chandra X-ray Observatory's article [8]). It was 400 times brighter than its usual quiet state (quiescence) and 3 times brighter than the previous brightest X-flare observed in 2012. After the giant black hole settled down, another extreme bright flare was observed a year after in October 2014. This flare was 200 times brighter than quiescence. These recent events are an opportunity to understand more the flaring mechanism of Sgr A* and other supermassive black holes. Astronomers have two theories about what caused these extreme flares. The first is from the theory of the asteroids explained above and illustrated by Figure 1. A gigantic asteroid would have been torn apart, after penetrating the hot region, as it was going around the black hole for couple of hours (which

¹the normal relatively quiet state of the black hole

²Fred Barganoof compares it to a water circling an open drain

correspond to the duration of the brightest flare) before passing the point of no return. ². If the theory holds and the cause of this enormous flare is really an asteroid, astronomers have found the largest asteroid responsible for an observed flare. The second theory is that magnetic field lines among the gas flow around Sgr A* could get tangled and occasionally reconfigure themselves and reconnect. These types of magnetic flares are often seen on the sun and Sgr A* flares present similarities in patterns of intensity with the flares from the Sun.

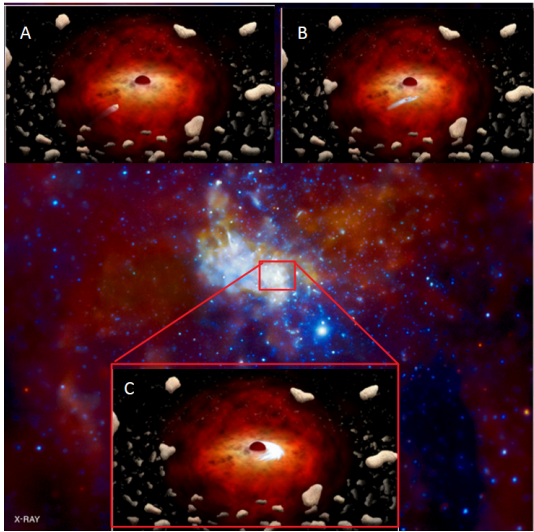


Figure 1: X-ray Image in the center of the Milky Way where red, green, and blue represent low, medium, and high-energy X-rays detected by Chandra X-ray Observatory. Three artistic pictures describe the theory of flare production from asteroids falling in Sgr A*. Panel A: Asteroid heading towards black hole. Panel B: Tidal forces tear up asteroid. Panel C: Asteroid is vaporized and flare occurs (Modified picture originating from [6]). Credit: NASA/CXC/Northwestern Univ/D.Haggard et al

For the purpose of this research we are trying to

study the variability in the signal , received from the X-ray source, to detect flares in 900 ks of data between May 2013 and October 2014. The two gigantic flares discussed above occurred in this period. We use the Bayesian blocks (bblocks) algorithm, developed by J.Scargle, to study the variability of the signal. When it was first developed (Scargle 1998 [11]), the algorithm was a very rough approximation. While they were improving the algorithm, intermediate papers came out in 2001 and 2003 until a final version of the improved algorithm came out in 2013. The version in preparation was implemented in a software called Interactive Spectral Interpretation System (ISIS) to perform the analysis on lightcurves, which are plots of the count rates of the photons received as a function of constant binned time. The scientist Peter K.G. Williams created a python kit that follows the last version of the improved algorithm released in 2013. In this paper, we try to present these two versions of the Bayesian blocks algorithm and use it to search for flares in 900 ks data. We also compare our results with those found in the G.Ponti 2015 [2] paper. We hope to end up with similar results with both ISIS and Peter Williams versions. Once we confirm (to a certain confidence level) the presence of flares, we hope that future research will be able to use it to improve their understanding of the mechanism of flares and solidify theories of the causes of the flares.

2 G2 object, magnetar SGR J1745-2900 and the increase of flaring rate.

Astronomers have been watching closely a strange object, of 3 Earths' worth of mass in gas, called G2 which made its closest approach to the supermassive black hole in late 2013. The object could be something else than just gas: like an exoplanet enveloped with gas. The nature of G2 as well as the hypothesis on the effects of G2's close passage on Sgr A* is discussed in Daryl Haggard and Geoffrey C. Bower for Sky and Telescope [3].

Since the past year, astronomers have noticed an increase in the flaring rate. NASA article [7] report that the newest set of observations "between August 30 and October 2014, revealed six bright flares within about three days, while an average of only 0.8 bright flares was expected". The Ponti paper [2] discuss this recent increase in the flaring rate. The timing roughly correspond to the close passage of G2 but some evidences (e.g., observations of similar behavior to this rise in other black holes) discussed in the Section "Inflows, Outflows and Flares" of the Sky & Telescope article suggest that G2 is not responsible for this rise in the flaring rates. It is possible that this increase is a common thing for supermassive black holes. However if G2, were responsible, it could be explained as so: the gravity of Sgr A* would have attracted some of the gas from the object onto the black hole and, with this excess material interacting with the hot gas of the accretion disk, would have created more frequent flares. During this intense monitoring of G2 passage near the black hole, astronomers made the

discovery of a compact object 0.3 light-years away from the black hole emitting pulses of X-ray every 3.6 seconds. This object, SGR J1745-2900, is called a magnetar.

3 Observations

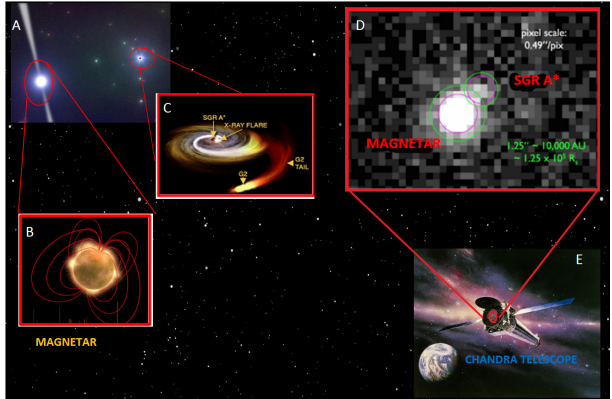


Figure 2: The observation technique of Sgr A*. Panel A: an image of Sgr A* and the magnetar SGR J1745-2900. Panel B: the artistic picture of a magnetar and its strong magnetic field lines. Panel C: An artistic picture of Sgr A* and the object G2 during its close approach potentially causing the flare (theory not proven). Panel D: An X-ray image from Chandra Observatory observed during the brightest flare showing the black hole and the magnetar flares from which we sort the photon data by their source

In this section we present briefly some of the technique to collect and isolate the X-ray photons coming from Sgr A* (and not from other X-ray background sources). The observations come from the Advanced CCD Imaging Spectrometer (ACIS). It's an X-ray imager containing a camera which detects individually the X-ray photons and record their po-

sition, energy and arrival time. (See <http://cxc.harvard.edu/cal/Acis/>). Chandra uses two different CCDs in this Chandra monitoring Campaign (ACIS-I and ACIS-S) (See M.A Nowak 2012 [9] and G. Ponti 2015 [2]). ACIS can be used with the High Energy Transmission Grating (HETG) (See http://space.mit.edu/HETG/hetg_info.html as well as M.A Nowak 2012 [9] and G. Ponti 2015 [2]). The data is then digitalized and reduced using the standard tools from CIAO analysis suite, version 4.6. (Neilsen 2013 and Nowak 2012).

The photons from Sgr A* are extracted from a region with radius 1.25 arcsec. This correspond to $\sim 10000AU$ and $\sim 1.6 \times 10^5 R_g$. where R_g is the black hole gravitational constant. The magnetar, SGR J1745-2900, is located $\sim 2.4arcsec$ from Sgr A*. This X-ray source contaminates the observations of Sgr A*(see PanelD in Figure 2). Periods of high background activity are filtered out. As mentioned in Section 2.2 of Ponti 2015: after the appropriate work of filtering , "less than $\sim 3\%$ of the flux from SGR J1745-2900 contaminates the extraction region of Sgr A*."

4 Theory and the algorithm

4.1 The basics of the Bayesian Blocks technique

Our objective in this section is to provide some background on how the Bayesian blocks algorithm described in Scargle 2013 [13] works. The first goal of the algorithm is to find the "change points" in our data. Change points are times in the data where the

variability of the flux (or count rate) is significant. The data we collect are time events. Each time event is the representation of a photon hitting a detector (for example, one of the CCDs on the Chandra's X-ray Observatory) . A lightcurve is the representation of the number of counts (or flux, or count rate) that occur in a constant binned time interval (300s in our case). The data that we receive contains observational errors which appear in the lightcurve as a noisy signal. The change points are the places in the data where we believe a significant change happened in the data not because of observational errors but because of the source. The first step of the algorithm is to make the problem of finding the change points finite by dividing the data into cells of different widths. The algorithm seeks a change point in a discrete interval instead of a continuous time interval. (Section 3.1 of Scargle 2013 [10] and Section 2.2 of Scargle 2013 [13])³. The block representation of the Bayesian Blocks (bblocks) considers the count rate (or flux) between two change points as constant and each change point represent the end of a block and the start of a the next block (except in the case of the first and last change points). For example, at the top of Figure (1) in Appendix A, the lightcurve (in green) is very noisy, but the variability of the lightcurve is more significant at some time points. At the time points where the algorithm decides that the variability is significant, it creates a change point and block with a width from one change point to the next. The height of the block is the signal intensity "averaged over the interval" (Section 2.3 of Scargle 2013 [13]). The next section explains how the algorithm chooses the best arrangement of blocks.

³The algorithm seeks which cell present a change point instead of which point in a continuous interval present a change point

4.2 The Fitness function

An observation interval I can be represented by different partitions P (i.e., different set of blocks adding up the whole interval). The algorithm tries to find the right partition (or model) among all the piecewise-constant models. The algorithm does this by maximizing the quantity that measure the fitness of the model. (Section 2.4 and Section 3 of Scargle 2013 [13]). As described by Section 2.4 of (Scargle 2013 [13]) the fitness function of the model must be "block-additive". It must respect this equation:

$$F[P(I)] = \sum_{k=1}^{N_{blocks}} f(B_k) \quad (1)$$

where $f(B_k)$ is the fitness of a block k and $F[P(I)]$ is the total fitness of the partition P over an interval I . We want to maximize F over all the partitions which indicate which cells belong to a certain block. ⁴

In section 3 of Scargle 2013 [13], there is an example of a fitness function that applies to our case of event data, but he also encourages the reader to explore other block-additive fitness functions. The example that he uses is a fitness function starting with the "unbinned likelihood known as the Cash statistic." For a single block, the model is constant and only has one parameter $M(t, \lambda) = \lambda$. For a block k the unbinned likelihood is derived as:

$$\log L^{(k)}(\lambda) = N^{(k)} \log \lambda - \lambda T^{(k)} \quad (2)$$

where $N^{(k)}$ is the number of events in block k and $T^{(k)}$ is the length of the block.

This likelihood is maximum for $\lambda = N^k / T^k$. So

⁴Again, the cells make the problem finite. A block is a grouping of cells and we want to find the right cell groupings to form the best block segmentation of the data.

we have:

$$\log L_{max}^{(k)} + N^{(k)} = N^{(k)} (\log N^{(k)} - \log T^{(k)}) \quad (3)$$

where N^k on the left side is model-independent and therefore irrelevant. This fitness function of a block k is block-additive and allows us to use equation (1) to find the optimum representation of our data.

The algorithm includes two very important parameters: ncp_prior controls the number of blocks representing the data and p_0 is the false positive rate (i.e., probability of falsely detecting a change point). Section 3 of Scargle 2013 calibrates ncp_prior from simulations of signal-free observational noise (more details in section 2.7 of Scargle 2013 [13]). After extensive simulation they arrive at a good calibration of ncp_prior with the formula:

$$ncp_prior = 4 - 73.53 p_0 N^{-0.478} \quad (4)$$

Peter Williams (PW) uses a different ncp_prior formula:

$$ncp_prior = 4 - \log\left(\frac{p_0}{0.0136 * ncells^{0.478}}\right) \quad (5)$$

where $ncells$ is defined by PW to be the number of input cells/bins which we supposed corresponds to the number of cells created from the event data. (more details in the source code of PW that can be found at http://pwkit.readthedocs.io/en/latest/_modules/pwkit/bblocks/#bin_bblock)

5 Two versions of the algorithm

5.1 PW kit

Peter K.G Williams (PW) developed a kit in python (that can be found on his website <http://pkit.readthedocs.io/en/latest/science/pkit-bblocks/>) following the technique described in Scargle 2013 [13]. Once the kit is imported in python we use the command `< pkit.bblocks.tt_bblock>` or `< pkit.bblocks.bs_tt_bblock>` depending on which mode we use. There are 3 modes in his kit that can output blocks. The two that we care about are the "normal event mode" and the "bootstrap event mode". Both require an event time array as the input of the command. The normal mode doesn't give any information on the error. The bootstrap mode is a technique that PW uses to get an estimate of the error on the count rate of the blocks. But he notes it's still a rough estimate. In order to have some intuition on the error of the blocks rates, we primarily use the bootstrap version in this paper. The inputs and outputs of these two modes are found in Appendices B and C. For all the plots in this paper we used a value of the false positive rate (i.e probability of falsely detecting a change point) to be $p_0 = 0.05$ (a slightly different value than the J.Neilsen 2013 paper [4]). According to Mossoux 2015 [1], our choice for p_0 implies that the probability that a change point found is a real one is $1 - 0.05 = 95\%$ and the probability that a flare (so two change points) is "a real flare" is $1 - p_0^2 = 99.75\%$. We provide all the data files and codes needed to create the plots in this paper. We created a code called `peter_williams.py` using PW's kit to plot the bblocks on top of the Sgr A*

lightcurves. The code asks for the Chandra ObsID, a value for p_0 and the mode (normal or bootstrap). The code then plots the lightcurve of the corresponding Chandra ObsID and the bblocks on top of it (see figure 4).

5.2 ISIS' script

The script that we use to plot Bayesian blocks with ISIS is called "bblocks_examp.sl". The instructions to get this file and use the script to plot Bayesian blocks can be found at http://space.mit.edu/cxc/analysis/SITAR/bb_examp.html. The example script, written by M.A Nowak, takes the fits file containing the data as an argument and a value of `ncp_prior`. It outputs the necessary data to plot the blocks: the start and stop times of the different blocks, the rate of each block and also the Poisson error on each rate. It uses the function `< sitar_make_data_cells()>` to make the cells and then uses the function `<sitar_global_optimum()>` to output the Bayesian blocks. All the outputs are presented in Appendices D and E. The prior parameter, `ncp_prior`, is required as an input in the script: it controls the number of blocks output with a general significance level value. The algorithm that ISIS uses is older than the Scargle 2013 [13] paper. It uses intermediate papers and conferences (see Scargle 2001 [12]). It gives a segmentation of the data for a given significance value (or confidence level). However this result is a rough estimate and should be followed by a series of Monte Carlo simulations (beyond the scope of this paper). In this paper we first use the PW kit and then use the ISIS version to check that the results coincide.

6 Results

6.1 Flare Detection

We looked for flares in 28 observations between May 2013 and October 2014. Figure 5 plots all the lightcurves stacked together (deleting the gaps between observations) at the top and the Bayesian blocks at the bottom. That means that we ignored the times when there was no observations and we pretend that it was a continuation. The reader should be aware that where there are vertical red lines, time has elapsed during which we do not know what the signal look like. Figure 5 displays the presence of two bright flares and some faint flares reported in Table 3 from PW analysis. The very bright flare of ObsID 16218 is almost a factor of two fainter than the brightest flare ever observed from Sgr A* at X-ray wavelengths. The peak count rate of this very bright flare is $0.45 \pm 0.04 \text{counts/s}$ while the peak count rate of the brightest flare is $0.87 \pm 0.07 \text{counts/s}$. The very bright flare of ObsID 16218 is found at the end of all the observations. It is followed by a subflare of count rate $0.044 \pm 0.016 \text{counts/s}$.

During these 18 months of observation, there are flares much fainter. We reported the faint flares found by both ISIS method (see Table 2) and PW method (See Table 3) and we also reported those discovered in G.Ponti's paper [2] (see Table 4). In Table 1 we use the python version of the Bayesian blocks algorithm from PW to find these flares. We run the algorithm for every ObsID (which give us figures similar to Figure 3 and Figure 4) with the false positive rate $p_0 = 0.05$. We consider then as flare, the blocks

which are approximately 2σ above the smallest block rate of the blocks segmentation of the particular observation (i.e., the quiescent level). To stay consistent we take the liberty to judge according to the graphs⁵ if a block, that is 2σ above quiescence, is not a flare. Often it's because there are large blocks near a high narrow flare that are accompanying the flares but aren't flares. Another concept/choice, concerning the flares definition, is that we observe some times like in Figure 3 or Figure 4 that a big flare can be divided in sub-blocks. We don't consider these substructures as flares but we do report them in Table 1. The choice of defining a block to be a flare is pretty open and is an approximation especially since the errors of the blocks rates are not very good estimations according to PW. We use the ISIS version of the algorithm from the script developed by M.A. Nowak to confirm the detection of flares that we found with the PW python version and we report the flares found in Table 2 with the significance value at which we detected the particular flares (most were detected at at least 99% and few of them at at least 95% significance). We plotted all the graphs with ISIS and PW and used the output data to report and compare the flares from both techniques. Figure 1 in Appendix A, present some of the most important faint flares found both with PW and ISIS for significance levels of 99.83% and 99.9%. However a Monte Carlo simulation should be done to come to a much better estimation of the confidence levels and detection of true flares. One can use Table 2, 3 and 4 to compare the results of both ISIS and PW methods and to also compare with the results from G.Ponti [2]. In these tables, the values in red are the values that are present in only one of the three sim-

⁵all the graphs for ISIS and PW will be provided with this paper as a zip file

ObsID	Obs Start (MJD)	Exp. (s)	Bg_rate (s)	Flare start (UT)	Flare stop (UT)	Rate (count/s)	Duration (s)
14702	484742330	13668	0.00066667	1500	4562.2011278	0.021±0.004	3062.2011278
15040	485869117	23750	0.0027854
14703	486722716	16840	0.00979798
15651	486855158	13752	0.00037037
15654	487139176	9028	0.00090802	7709.10441151	11700.	0.0045±0.0010	3990.89558849
14946	489134984	18202	0.0077451
15041	491275637	45410	0.00412164	7382.38815305 34500	8424.11288476 35333.64574081	0.035±0.012 0.032±0.017	1041.72473171 833.64574081
15042	492649078	45674	0.00714262	34200	45539.82110092	0.019±0.008	11339.82110092
14945	494331166	18201	0.00765258
15043	495504292	45410	0.00947377	7022.74001792 7485.82632825 7811.08929104 8941.01955768 8941.01955768 9175.8703706 10336.01124388 11456.89991516	7485.82632825 7811.08929104 8941.01955768 9175.8703706 10336.01124388 11456.89991516 12561.47027045	0.17±0.04 0.49±0.12 0.87±0.07 0.43±0.19 0.81±0.04 0.35±0.03 0.10±0.02	463.08631033 325.26296279 1129.93026665 234.85081291 1160.14087328 1120.88867128 1104.5703553
14944	496047776	18202	0.00555556	14086.69902754	16500	0.02±0.01	2413.30097246
15044	497294688	42688	0.00827083
14943	498411665	18202	0.00693578	1200.	3156.61825415	0.015 ±0.007	1956.61825415
14704	498905670	36341	0.00561905
15045	499357874	45410	0.00702553	6000 19500	8400 20473.95916006	0.03±0.01 0.03±0.01	2400 973.95916006
16508	509369868	43414	0.00346988	47100	48647.22380629	0.027±0.009	1547.22380629
16211	511179507	41783	0.00842887
16212	512965587	45411	0.00819608
16213	515040305	44955	0.00788955
16214	516932351	45409	0.00686047
16210	518151563	17022	0.00677083
16597	520894092	16464	0.00360656
16215	521937832	41453	0.00634409
16216	523337501	42689	0.00529405
16217	525761412	34526	0.00227273	25102.29492405	29700	0.02±0.01	4597.70507595
16218	530180548	36340	0.00595322	17805.50359073 18951.30951434 19320.2343049 20217.73818475 20811.1492027	18951.30951434 19320.2343049 20217.73818475 20811.1492027 21126.04736018	0.061±0.015 0.17±0.07 0.45±0.04 0.26±0.07 0.10±0.05	1145.80592361 368.92479056 897.50387985 593.41101795 314.89815748

Table 1: List of 26 observations including the flares (we give the feature of the flare when we have one or we use "..."). The blocks are considered flares if they are 2σ away (higher) than the smallest block rate in each observation. The table provide for the start time of the observation, the exposure, the background rate (the rate of the smaller block in the block segmentation of the data), the start and end time of the flare, the rate of the block representing the flare and the duration of the flare. The observation ID are not in ascending order.)

ulations, the dark blues values are the flares present in both PW and ISIS methods and the light blue are the values present in both ISIS analysis and Ponti's work. We are able to conclude for all the flares and faint flares discovered by this analysis and to accept or reject some of the flares based on these different simulations (for example if we discover a very small flare with a big error only appearing in one simulation we can decide to reject it). The reader should notice that ISIS and PW versions seems to present some minor differences on the lightcurve they output: ISIS doesn't include the binned where no photons are detected if it's at the beginning or the end of the observations where PW kit does. The other minor difference would be with the rate of some binned time that do not coincide. We think that this minor difference is not very relevant for the purpose of finding flares but should be noticed.

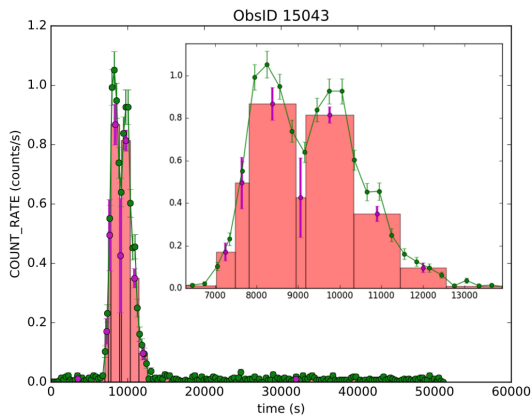


Figure 3: The block segmentation of the brightest flare found during the 18 months of observation using PW version of bblocks.(ISIS plot for this observation can be found in Appendix E). At the top right is a zoom on the flare.

⁶Two observations, ObsIDs 14941 and 14942, couldn't be evaluated with the rest of the data. Both observations didn't present any flare.

6.2 Flare Characteristics

6.2.1 Very bright flares

During the 18 months of observations (not taking into account the 2 ObsIDs from which I couldn't evaluate the data with the rest)⁶, plotted at the top of Figure 5, we can clearly see that there are two very bright flares in the data. The first very bright flares with ObsID 15043 is known as the brightest flare ever observed by Chandra in the X-ray domain. We found a peak rate of $0.87 \pm 0.07 \text{counts/s}$ for this observation, which is exactly the same block peak rate that was found in G.Ponti 2015 [2] (see table 6 in their paper). Figure 3 shows its plot using PW and Appendix E (Figure 2) shows the plot using ISIS at a significance level of 99%. This is almost twice as large as the other very bright flare that we found in ObsID 16218(see Figure 4 and Appendix E (3)). We found a peak rate of $0.45 \pm 0.04 \text{count/s}$ for this second bright flare. This peak rate was found to be $0.46 \pm 0.07 \text{count/s}$ in table 6 of G.ponti 2015 [2]. This very bright flare is followed by a subflare of block rate $0.044 \pm 0.016 \text{count/s}$ (see Figure 4). The block rate of this subflare was found to be $0.046 \pm 0.016 \text{count/s}$ in G.Ponti 2015. Sometimes wide and bright flares are divided into multiple blocks. It is the case for the two very bright flares found in this paper. In the Table1 all the blocks that divide the very bright flares of ObsID 15043 (very bright flare 1) and ObsID 16218 (very bright flare 2) are detailed. Very bright flare 1 is composed of 7 blocks and very bright flare 2 is composed of 5 blocks. The start and end time of the very bright flare is defined with the start time of the

first block that compose it and stop time of the last block.

6.2.2 The faint flares

In the 28 observations that we analyzed, if we do not count the two very bright flares, their substructure or their sub-flares, we found 15 faint flares using ISIS technique and 11 faint flares with PW technique while Ponti's work [2] led to only 9 faint flares. If we consider all the simulations and decide to accept all flares found as flare we end up with 16 faint flares. ISIS found all the flares that were found in Ponti's work and with PW's version except for the faint flare of Obs15654, found with PW, with block rate 0.0045 ± 0.0010 (see red value in Table 3). The flares that were found with our analysis but not in Ponti's work are in red and dark blue. That is the faint flares of ObsIDs 15041(one of them), 15042(two of them), 14945, 14704, 16211, 15654, 15041(one of them). They have blocks rates values of 0.038 ± 0.009 (15041), 0.029 ± 0.005 (15042), 0.032 ± 0.004 (15042), 0.0029 ± 0.008 (14945), 0.037 ± 0.0010 (14704), 0.040 ± 0.016 (16211), 0.0045 ± 0.0010 (15654) and 0.032 ± 0.0017 (15041) (all these values have units of count/s). Among these 8 faint flares not present in Ponti's work two of them present reasons to doubt that they should be excluded as flares: the faint flares of ObsID 14704 and 16211 because they were only found with ISIS and with a lower significance (95%). We also have doubts that the faint flare of ObsID15654 is really a flare because of its very small count rate value (i.e., 0.0045 ± 0.0010 count/s) and the fact that it was only found with PW version. Therefore we are pretty confident that we found 13 to 16 faint flares among which 5-8 of them

where not found in Ponti's work. A Monte Carlo simulations should be done to have stronger confidence on the actual number of flares found.

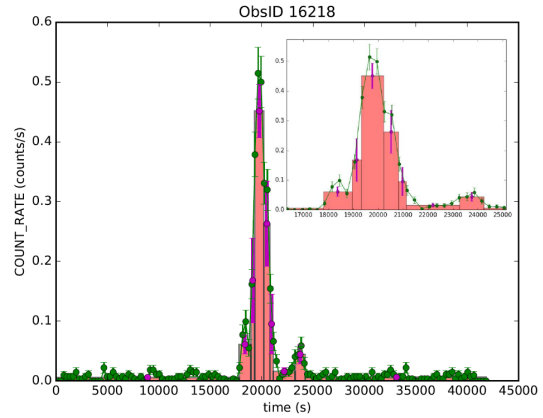


Figure 4: The block segmentation of the second brightest flare found during the 18 months of observation using PW version of bblocks. ISIS plot can be found in Appendix E.)

ObsID	Rate (count/s)	Sig (%)	ObsID	Rate (count/s)	Sig (%)
14702	0.0236 ± 0.0033	99	14944	0.023 ± 0.004	95
15041	0.04 ± 0.01 0.038 ± 0.009	99	14943	0.025 ± 0.006	99
15042	0.026 ± 0.007 0.029 ± 0.005 0.032 ± 0.004	99	14704	0.037 ± 0.010	95
14945	0.029 ± 0.008	99	15045	0.035 ± 0.005 0.034 ± 0.007	99
15043	0.184 ± 0.024 0.531 ± 0.045 0.87 ± 0.02(peak) 0.46 ± 0.03 0.26 ± 0.03 0.11 ± 0.01	99	16508	0.033 ± 0.006	99
			16211	0.040 ± 0.016	95
			16217	0.021 ± 0.002	99
			16218	0.067 ± 0.009 0.18 ± 0.03 0.44 ± 0.02(peak) 0.15 ± 0.02 0.05 ± 0.01(sub)	99

Table 2: Table of the flares found with ISIS analysis. (This analysis needs Monte Carlo simulations))

ObsID	Rate (count/s)	ObsID	Rate (count/s)
14702	0.021±0.004	14943	0.015 ±0.007
15654	0.0045±0.0010	15045	0.03±0.01
15041	0.035±0.012		0.03±0.01
	0.032±0.017	16217	0.02±0.01
15042	0.019±0.008	16508	0.027±0.009
14944	0.02±0.01		

Table 3: Table of the 11 faint flares found with our analysis.)

ObsID	Rate (count/s)	ObsID	Rate (count/s)
15041	0.037±0.013	14943	0.022 ±0.008
...		15045	0.033±0.008
15042	0.014±0.007		0.031±0.015
14945	0.0256±0.009	16508	0.024±0.006
14944	0.022±0.008	16217	0.020±0.004

Table 4: Table of the 9 faint flares found in G.Ponti 2015 for the same ObsIDs)

7 Discussion and Conclusion

As stated in Neilsen paper[5], we are close to understanding the physics of flares. We must continue the observations of Sgr A* to arrive finally one day to a solid conclusion for the causes of flares. The close passage of G2, around which the observations in this report are made, was a good opportunity to watch

and analyze Sgr A* signal variability and make discoveries. The results found in this report don't allow us to draw any direct conclusions about the mechanism and physics of flaring but we hope that these results can be used in the future and compared to other models to help for the quest to the understanding of flaring mechanisms. To go further in this research one can find a way to find more precise error values for the block rates found with the bootstrap method of Peter Williams and also implement the Monte Carlo simulations for the ISIS method to have more precise errors and significance value.

8 Acknowledgment

I want to thank Peter Williams and M.A Nowak for answering emails. I want to specifically thank my colleague and friend Jacky Van (computer science major), for helping in programming and computer related things. I want to thank my friend and housemate Jesutoni Olasubulumi for helping running repetitive tedious last minute code. I want to acknowledge my colleagues Brayden Mon, Noelia de la Cruz Hernandez, Gaylor Wafflard-Fernandez and Daniel Capellupo. And of course a special thank you for my supervisor, Daryl Haggard for supervising and supporting this report.

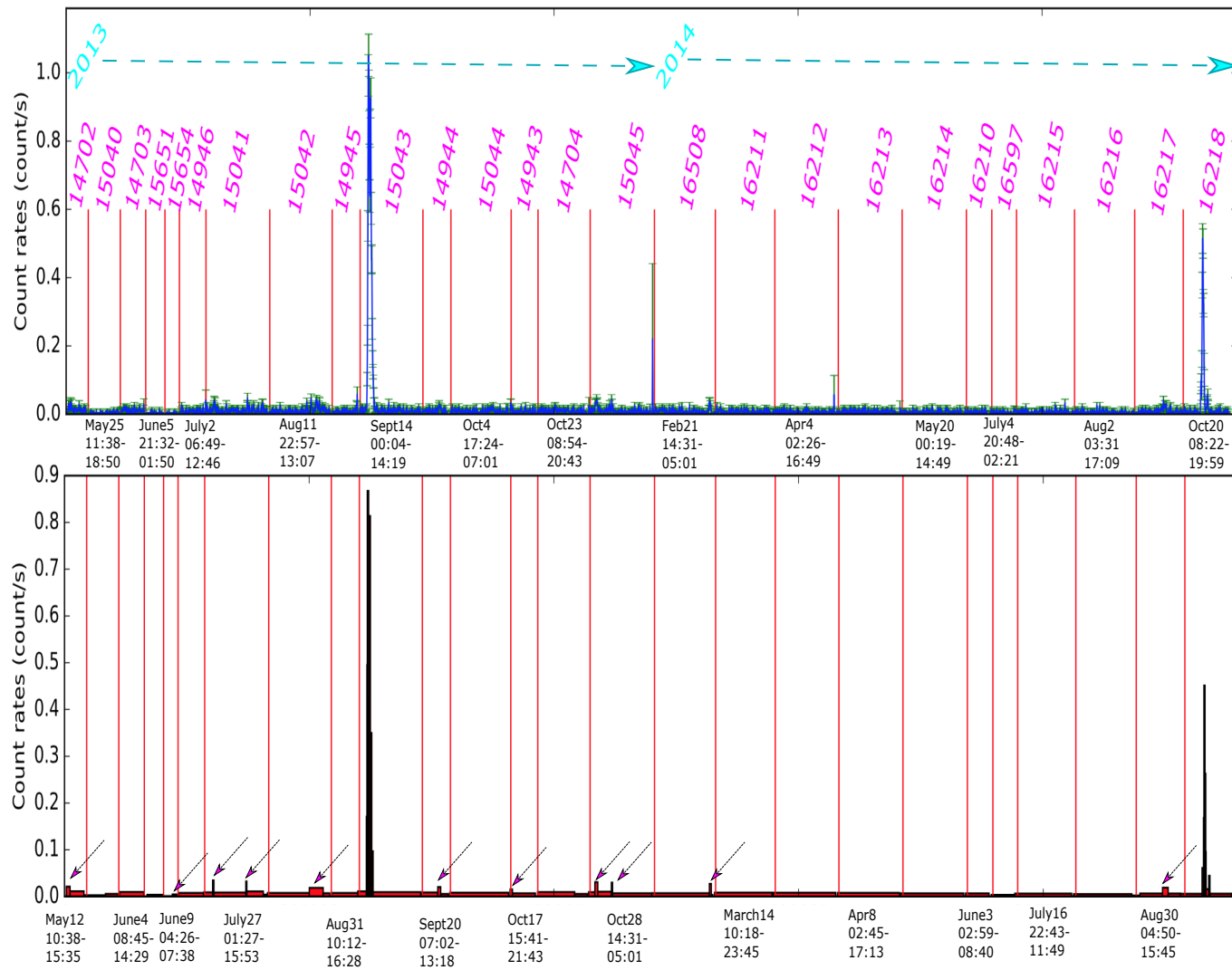


Figure 5: (Part1)Top: The lightcurve of 26 observations of SgrA* stacked together. The red line represent the beginning and end of the different observations and the line where two observations were stucked together ignoring the gap time during which there was no observation. Top pink number = ObsID ; Bottom number: start date of the observation with time range of the observation. Bottom: The Bayesian blocks with PW's version of the 18 months of observation. The arrows show the flares found with the bblocks from PW's version.

9 Appendix

A: The biggest of the small flares

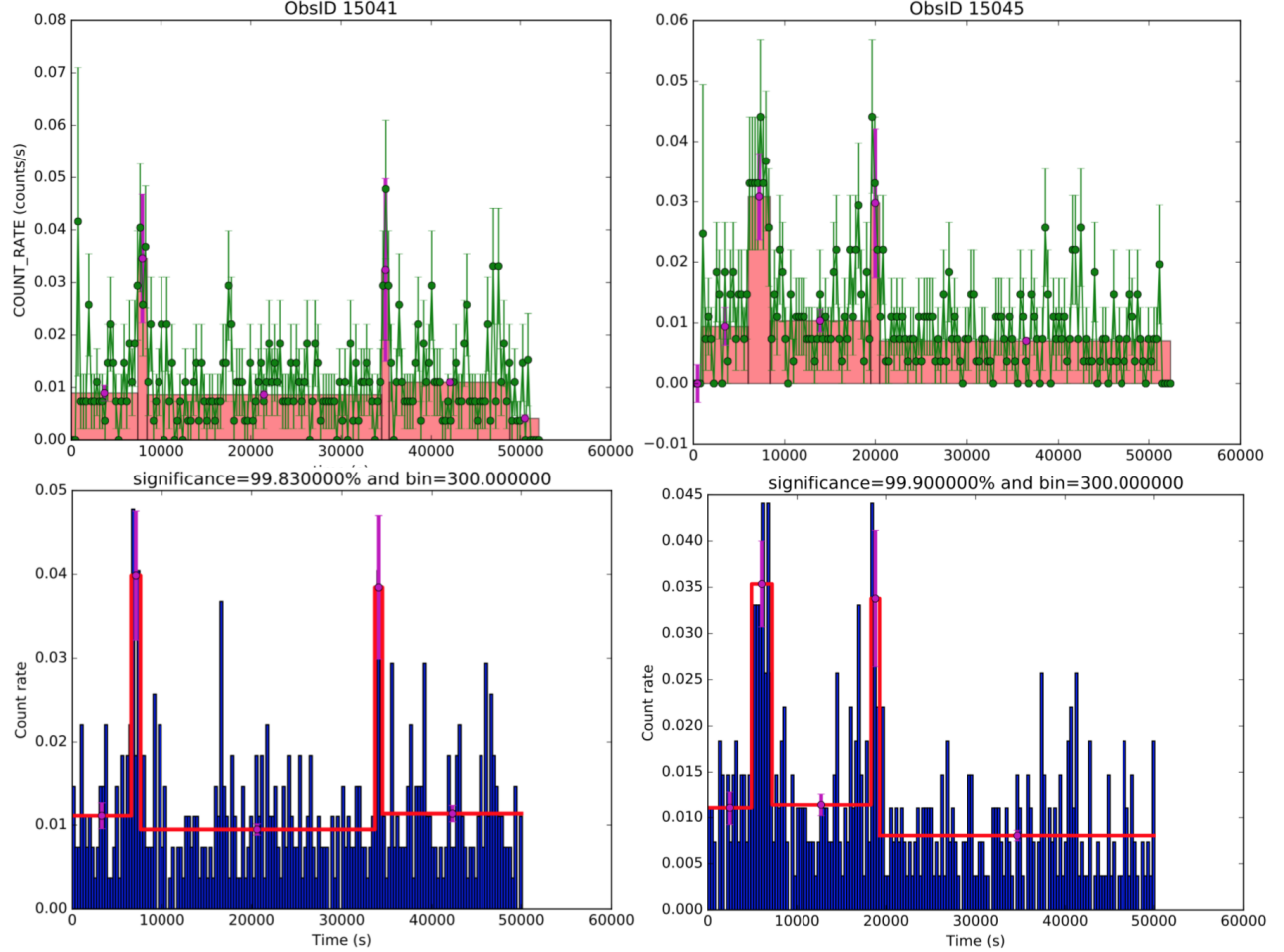


Figure 1: Two of the biggest faint flares found with observation ID 15041, 15045. Top left : PW bootstrap version for ObsID 15041. Top right: PW bootstrap version for ObsID 15045. Bottom left and right : ISIS version plotted with python for respectively ObsID 15041 and ObsID 15045. The lightcurve In PW version (in green) is represented as data points at the middle of 300s bins . The lightcurve in ISIS version (in blue) Is represented by bar plots of 300s bins. The purple error bars are estimates of the error of the flare rate represented by the block height. (According to Peter Williams, its errors bars are not very good error estimation)

B: Inputs and outputs for python version in normal mode

Inputs:

tstarts	Array of input bin start times
tstops	Array of input bin stop times
times	Array of event arrival times
p0=0.05	Probability of preferring solutions with additional bins

Outputs:

blockstarts	Start times of output blocks
counts	Number of events in each output block
finalp0	Final value of p0, after iteration to minimize 'nblocks'
Ledges	Times of left edges of output blocks
midpoints	Times of midpoints of output blocks
nblocks	Number of output blocks
ncells	Number of input cells/bins
origp0	Original value of p0
rates	Event rate associated with each block
redges	Times of right edges of output blocks
widths	Width of each output block

C: Inputs and outputs for python version in bootstrap mode

Inputs:

tstarts	Array of input bin start times
tstops	Array of input bin stop times
times	Array of event arrival times
p0=0.05	Probability of preferring solutions with additional bins
nbootstrap=512	Number of bootstrap runs to perform

Outputs:

blockstarts	Start times of output blocks
bsrates	Mean event rate in each bin from bootstrap analysis.
bsrstds	~Uncertainty: stddev of event rate in each bin from bootstrap analysis
counts	Number of events in each output block
finalp0	Final value of p0, after iteration to minimize 'nblocks'
Ledges	Times of left edges of output blocks
midpoints	Times of midpoints of output blocks
nblocks	Number of output blocks
ncells	Number of input cells/bins
origp0	Original value of p0
rates	Event rate associated with each block
redges	Times of right edges of output blocks
widths	Width of each output block

D: Description of the function < `sitar_make_data_cells()`>

Inputs:

<code>tt</code>	times of the detected events
<code>type</code>	Describe cells as "events" (type=1 or 2), with the size (i.e., normalized duration) being the distance from halfway from the previous event to halfway to the next event (type=1), or from the current event to right before the subsequent event (type=2). (Note: all cell populations are greater than or equal to one, and the total number of cells is less than or equal to the total number of events.) Alternatively, events can be assigned to bins of uniform size (type=3). (For this case, cells can have zero population, and the total number of cells can greatly exceed the total number of events.)
<code>max_delt</code>	Events closer together than <code>max_delt</code> are grouped together in a single cell. (Note: this is for grouping of <i>consecutive</i> events, such that the resulting cell duration can be greater than <code>max_delt</code> .)
<code>frame</code>	The output cell sizes are in units of frame, or this is the bin size for type=3
<code>tstart</code>	Start times for creating the output cells
<code>tstop</code>	stop times for creating the output cells

Outputs:

<code>cell</code>	A structure with fields
<code>cell.pops</code>	an array of the number of events per cell
<code>cell.size</code>	the size (i.e. duration) of a cell in units of frame or the mean counts per bin (derived from the total lightcurve) in binned mode (type=3); <code>cell.lo_t,hi_t</code> - the start and stop times of the cell
<code>cell.lo_t</code>	Start times of the cell
<code>cell.hi_t</code>	Stop times of the cell
<code>cell.dtcor</code>	an array, <i>currently set to unity</i> , for storing "dead time corrections" (or "efficiency" corrections) of the cells. Must be changed externally to this subroutine, and currently only used insitar_global_optimum to deadtime correct the output rates of the resulting blocks.

E: Description of the function < `sitar_global_optimum()`>

Inputs:

<code>cell</code>	A structure, with <code>cell.pops</code> , <code>cell.size</code> , <code>cell.lo_t</code> , <code>cell.hi_t</code> , <code>cell.dtcor</code>
<code>ncp_prior</code>	Parameter for prior on number of 'blocks'
<code>Type</code>	Identical to type from <code>sitar_make_data_cells</code>
<code>More optional inputs</code>	check http://space.mit.edu/cxc/analysis/SITAR/func_bb.html for more infos

Outputs:

<code>results.cpt</code>	Array of change point locations for the maximum likelihood solution (indices are specific to the cell input)
<code>results.last, results.best</code>	(Diagnostic purposes only) Arrays of the location of the last change point and the associated maximum log probability
<code>results.cts</code>	Counts in each block
<code>results.rate</code>	Rate in each block
<code>results.err</code>	Poisson error for the block rate
<code>results.lo_t,hi_t</code>	Times of lower (\geq) and upper ($<$) block boundaries

E: The two very bright flares with ISIS at 99% significance

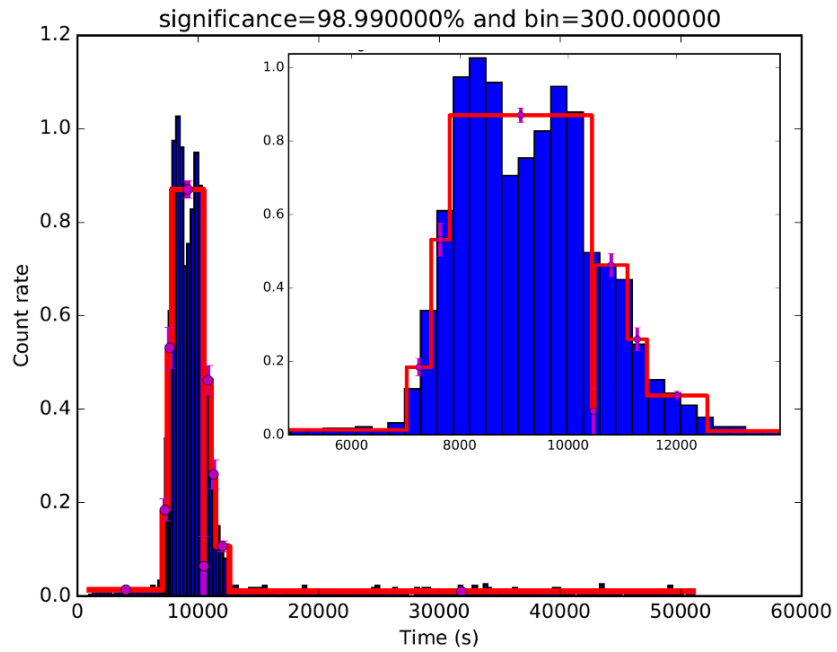


Figure 2: The brightest flare observed (in ObsID 15043) with ISIS analysis with 99% significance

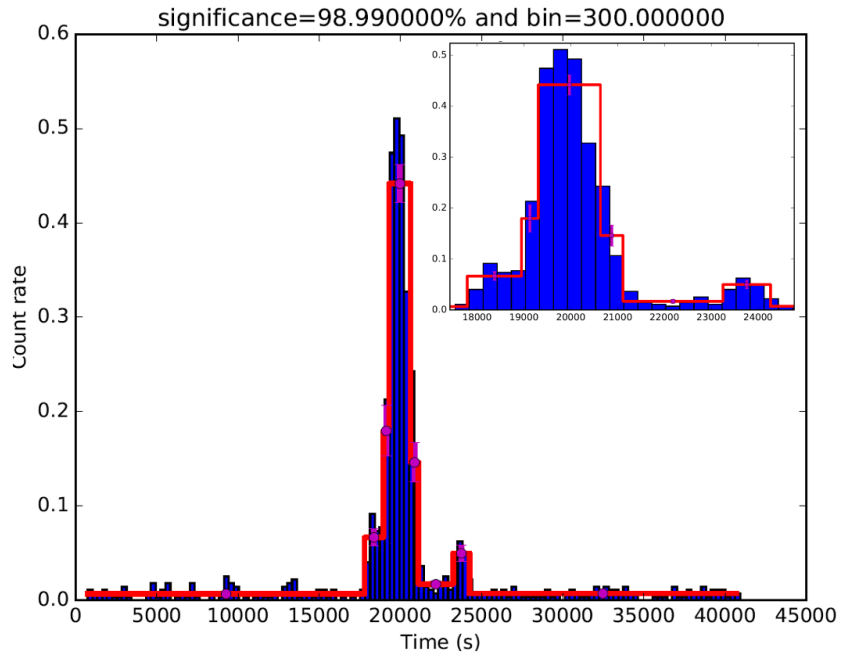


Figure 3: The second brightest flare observed (in ObsID 16218) with ISIS analysis at 99% significance

References

- [1] E.Mossoux. Study of the x-ray activity of sgra* during the 2011 xmm-newton campaign. *Astronomy and Astrophysics manuscript*, (24682), 2015.
- [2] G.Ponti. Fifteen years of xmm-newton and chandra monitoring of sgr a*: Evidence for a recent increase in the bright flaring rate. *doi:10.1093/mnras/stv1537*, (454), 2015.
- [3] Daryl Haggard and Geoffrey C. Bower. Into the heart of the milky way. *Sky and Telescope*, February 2016.
- [4] J.Neilsen and M.A Nowak. A chandra/hetgs census of x-ray variability from sgra* during 2012. *The Astrophysical Journal (apJ)*, (774:42), 2013.
- [5] J.Neilsen and M.A Nowak. The x-ray flux distribution of sagittarius a* as seen by chandra. *The Astrophysical Journal (apJ)*, (799:199), 2015.
- [6] NASA. Sagittarius a*: Nasa's chandra finds milky way's black hole may be grazing on asteroids. <http://chandra.harvard.edu/photo/2012/sgra/>, 2012.
- [7] NASA. Milky way's black hole shows signs of increased chatter. 2015.
- [8] NASA. Sagittarius a*: Nasa's chandra detects record-breaking outburst from milky way's black hole. <http://chandra.harvard.edu/photo/2015/sgra/>, 2015.
- [9] M.A Nowak. Chandra/hetgs observations of the brightest flare seen from sgra*. *The Astrophysical Journal (apJ)*, (759:95), 2012.
- [10] J. Scargle. Studies in astronomical time series analysis. vi. optimal segmentation: Blocks, triggers, and histograms. *Draft of July 11, 2006*.
- [11] J. Scargle. Studies in astronomical time series analysis. v. bayesian blocks, a new method to analyze structure in photon counting data. *The Astrophysical Journal (apJ)*, (504:405-418), 1998.
- [12] J. Scargle. Bayesian inference and maximum. Number 567, 2001.
- [13] J. Scargle. Studies in astronomical time series analysis. vi. bayesian block representations. *The Astrophysical Journal (apJ)*, (764:167), 2013.